JOURNAL OF GEOPHYSICAL RESEARCH, VOL. 103, NO. B3, PAGES 5019-5035, MARCH 10, 1998

Estimating horizontal gradients of tropospheric path delay with a single GPS receiver

Yoaz E. Bar-Sever and Peter M. Kroger

Jet Propulsion Laboratory, California Institute of Technology, Pasadena

Jorgen A. Borjesson

Onsala Space Observatory, Chalmers University of Technology, Onsala, Sweden

Abstract. We present evidence that modeling troposphere delay gradients in precise Global Positioning System (GPS) geodesy improves the accuracy and precision of the estimated quantities, and that the estimated gradients resemble real atmospheric moisture gradients observed with a water vapor radiometer (WVR). Using a low elevation angle cutoff, combined with a model of the atmospheric delay gradient as a random walk process leads to 19.5% and 15% average improvement in radial and horizontal site position repeatabilities, respectively, relative to a current state-of-the-art estimation strategy that does not model horizontal gradients and imposes high elevation angle cutoff. The agreement between estimated values of zenith wet delay from collocated GPS receivers and WVRs was improved by at least 25%. Merely lowering the elevation angle cutoff improves the repeatability of the radial component of the site's position vector but tends to degrade the repeatability of the horizontal components of the position vector if troposphere gradients are not properly modeled. The estimates of wet delay gradients from a collocated GPS receiver and a WVR at Onsala, Sweden, seem to be correlated over timescales as short as 15 min. The agreement in azimuth between the GPS-based and the WVR-based gradients was at the 10° level, for significant gradients. The GPS was found to under-estimate the magnitude of the gradients by about 60% relative to the WVR-based gradients. The ability to sense atmospheric moisture gradients from a single GPS receiver increases the useful information content from networks of GPS receivers by providing additional spatial information for weather forecasting applications.

1. Introduction

The Global Positioning System (GPS) reached operational status in early 1994 and is now operating continuously with the full 24-satellite constellation. An explosion in the number of applications has transformed the system from a mere navigation tool to a valuable remote sensing system. Traditionally used for high-precision geodesy, the GPS system has recently emerged as a powerful tool in atmospheric studies, in particular, climatology and meteorology. In fact, the geodetic and atmospheric applications of the GPS cannot be separated; to get the precise location of the receiver, the delay suffered by the GPS signal while traversing the atmosphere must be accurately known.

The main meteorological product of ground-based GPS is the estimate of precipitable water vapor (PW), the vertically integrated quantity of atmospheric water vapor. Using ancillary measurements of surface pressure and temperature, PW is inferred from values of total zenith delay (TZD) which are directly estimated from the GPS data. Its high temporal resolution, proven all-weather high accuracy and low cost, make ground-based GPS a uniquely powerful system for the observation of water vapor.

The TZD is the atmospheric delay of a GPS signal arriving from the zenith direction. It can be separated into two components, a delay due to the dry gases in the troposphere and the nondipole component of water vapor refractivity, denoted as zenith hydrostatic delay (D_{hz}), and a delay due to the dipole component of water vapor refractivity in the atmosphere, denoted as zenith wet delay (D_{wz}) [*Davis et al.*, 1985]. The zenith hydrostatic delay can be accurately inferred from precise measurements of surface atmospheric pressure using the formula:

$$D_{hz} = 0.22765P/(1 - 0.00266\cos 2\lambda - 0.00028h),$$

where P is surface pressure in millibars, λ is the latitude, h is geodetic height in kilometers, and D_{hz} is given

Paper number 97JB03534.
0148-0227/98/97JB-03534$09.00

Table 1. Differences Between Estimation Startegies

Estimation Strategy	Elevation Angle Cutoff, deg.	Sigma for D_{wz}, mm/$\sqrt{\text{h}}$	Sigma for G_N and G_E, mm/$\sqrt{\text{h}}$	Postfit Window, cm
Current JPL	15	10.2	Not modeled	5.0
Nominal homogeneous	7	3.0	Not modeled	5.0
Nominal inhomogeneous	7	3.0	0.6	5.0
Constant gradient	7	3.0	0.0	5.0
Tuned inhomogeneous	7	3.0	0.3	2.5
Tuned 15°	15	3.0	0.3	2.5

in centimeters [*Saastamoinen*, 1971]. After removing the hydrostatic component from the total delay, the remaining zenith wet delay is nearly proportional to the PW, the quantity of water vapor integrated along the zenith direction [*Bevis et al.*, 1994], that is,

$$PW = \pi D_{wz}.$$

The proportionality factor π is a weak function of T_m, the weighted mean temperature of the atmosphere column,

$$\pi = 10^6/(\rho R_v(k_2' + k_3/T_m)),$$

where k_2' and k_3 are empirical physical constants, ρ is the density of liquid water, and R_v is the specific gas constant for water vapor. *Bevis et al.* [1994] have derived the following regression formula to approximate T_m from values of surface temperature:

$$T_m = 0.72t + 70.2 \quad (°\text{K}).$$

The connection between the line-of-sight delay for the individual satellite-receiver link D_L and the zenith delay parameters, D_{hz} and D_{wz} is made through the "hydrostatic" and "wet" mapping functions $m_h(e)$ and $m_w(e)$, respectively, that is,

$$D_L = m_h(e)D_{hz} + m_w(e)D_{wz}, \qquad (1)$$

where e is the elevation angle, measured from the local horizon to the line of sight. Several such mapping functions exist, and the most commonly used in precise geodetic applications are those derived by *Lanyi* [1984], *Herring* [1992], and *Niell* [1996]. The zenith hydrostatic delay component D_{hz} typically accounts for about 90% of the total delay at any given site and, as mentioned above, is highly predictable based on surface pressure. The zenith wet delay, although relatively small (typically less than 30 cm), is highly variable and unpredictable. In precise GPS applications where millimeter accuracy is desired, the zenith wet delay must be estimated with the other geodetic quantities of interest.

The only variable in (1) is the elevation angle, revealing the underlying assumption that the atmosphere is azimuthally homogeneous. Azimuthally inhomogeneous mapping functions have been proposed as early as 1977 [*Gardner*, 1977] but have never been used in routine GPS geodesy, although a successful application of an azimuthally inhomogeneous atmosphere mapping function in very long baseline interferometry (VLBI) was reported by *Chen and Herring* [1997] and *MacMillan* [1995]. Several recent studies have pointed to mismodeling of the troposphere delay as one of the largest error sources in precise GPS geodesy [*Ware et al.*, 1997; *Bar-Sever*, 1996; *Heflin et al.*, 1996; *Heflin et al.*, 1994].

In this paper we evaluate the errors in geodetic applications caused by the assumption of azimuthal homogeneity in the troposphere mapping functions, and we present an improved model. We do so by adding to the

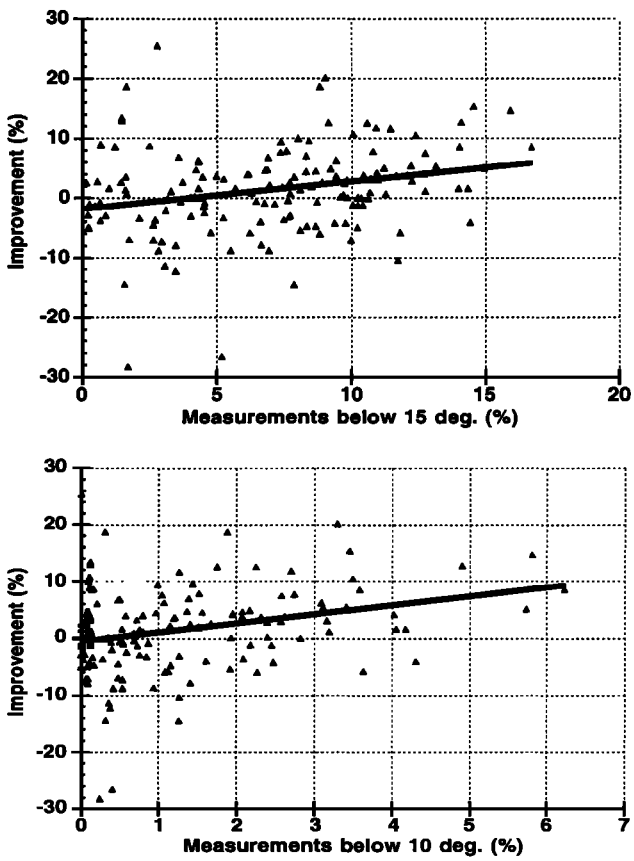

Figure 1. Improvement in 3-D position repeatability due to the nominal inhomogeneous strategy relative to the nominal homogeneous strategy, plotted as a function of the percentage of low elevation angle measurements, 149 IGS sites included. The mean improvement over all sites was 1.6%.

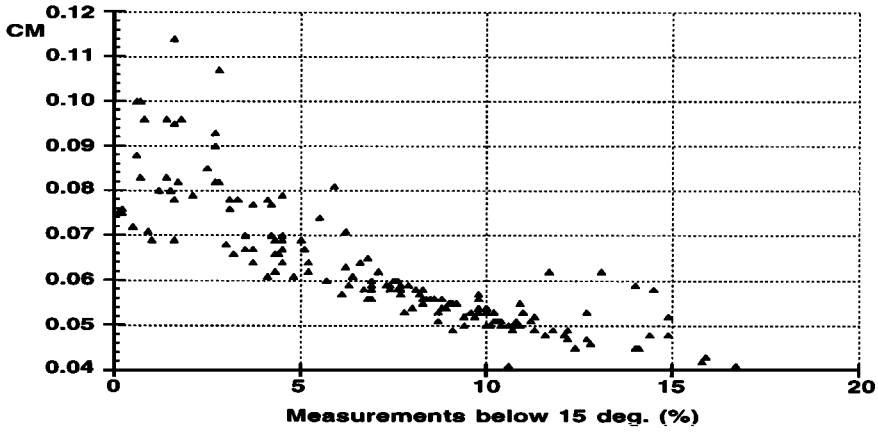

Figure 2. Median formal errors of the estimated gradients with the nominal inhomogeneous strategy as a function of the mean daily percentage of measurements between 7° and 15°. Nominal inhomogeneous strategy as a function of the mean daily percentage of measurements between 7° elevation angle cutoff was used. For each site the median was taken over all output epochs (every 5 min) during October - December 1996. The formal errors for the estimates of the position vector show a similar pattern. Three sites with very little data overall, and hence high formal errors, were excluded.

homogeneous mapping function a simple azimuthally dependent component representing a horizontal gradient in the tropospheric delay. We use the precise point positioning technique [*Zumberge et al.*, 1997] to demonstrate that under certain conditions, using the gradient model significantly improves important aspects of solution quality. In doing so, we address the controversial issue of low elevation angle tracking and present yet another piece of evidence in support of lowering elevation angle cutoff values despite the increase in multipath and the reduction in signal-to-noise ratio that accompanies low-elevation measurements. We also present preliminary results demonstrating that the observed gradients represent real atmospheric features and are not artifacts caused by other errors such as multipath and GPS orbital errors. Whereas the traditional estimation of zenith delay supplies one-dimensional vertical information, estimating the horizontal gradient adds information about the horizontal dimension. This increases the useful information content from networks of GPS receivers and increases the utility of ground-based GPS measurements for weather forecasting.

The gradient model is described in the next section, followed by sections describing the setup and results from a series of experiments designed to test the impact of the gradient model on precise point positioning. We then proceed to evaluate the accuracy of the estimated gradients using data from a water vapor radiometer (WVR). We end with a discussion of the results.

2. Gradient Model

Following *MacMillan* [1995], the delay in the GPS signal due to the troposphere gradient is modeled as

$$\Delta D = m_\Delta(e) \cot e[G_N \cos\phi + G_E \sin\phi]$$

where ϕ is the azimuth angle measured eastward from north. The reason behind the name "gradient model" can easily be seen if we rewrite the model as

$$\Delta D = m_\Delta(e) \cot e|G| < U_G, U_\phi >,$$

where $G = (G_N, G_E)$ is the gradient vector, $U_\phi = (\cos\phi, \sin\phi)$ is the azimuth vector, $U_G = G/|G|$, and angle brackets indicate an inner (dot) product. The magnitude of ΔD is greatest when the azimuth vector points along the gradient vector, and ΔD is zero when the azimuth vector is perpendicular to the gradient vector.

Together with the homogeneous terms the complete model for the line-of-sight delay is

$$\begin{aligned} D_L &= m_h(e)D_{hz} + m_w(e)D_{wz} \\ &\quad + m_\Delta(e) \cot e[G_N \cos\phi + G_E \sin\phi]. \end{aligned} \tag{2}$$

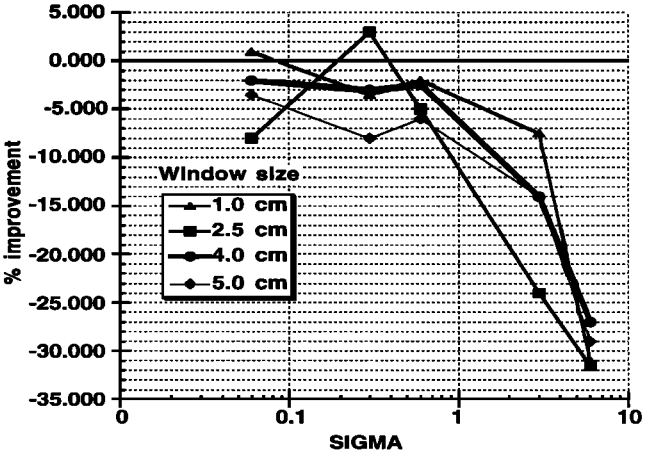

Figure 3. Tuning the estimation strategy for site AOA1 in southern California. Performance is measured as improved repeatability in the radial coordinate when comparing to the nominal homogeneous strategy.

Table 2. Mean Improvement in Position Repeatability due to Each Strategy

Strategy	Radial	Horizontal	Three-Dimensional
Nominal homogeneous	9.3	-3.7	5.4
Nominal inhomogeneous	13.4	2.6	10.2
Constant gradient	12.3	2.8	9.7
Tuned inhomogeneous	19.5	15.2	18.2
Tuned 15°	11.0	11.6	11.2

Improvement is measured relative to the current JPL strategy. Based on the 37 sites with more than 2% of all measurements between 10° and 7°. Units in percent.

We implemented this model in Jet Propulsion Laboratory's (JPL) GIPSY OASIS software where we chose m_h and m_w to be *Niell*'s [1996] hydrostatic and wet mapping functions, respectively. We chose $m_\Delta = m_w$ although the choice of m_h gave essentially the same results. *Chen and Herring* [1997] discuss an alternative inhomogeneous mapping function that avoids the singularity at zero elevation angle. They apply it to VLBI data and validate it by comparisons to three-dimensional weather analysis fields. We did not attempt to evaluate their mapping function here.

It is evident from (2) that observations from sufficiently low elevation angles are required in order to separate the gradient components from the azimuthally homogeneous components. *MacMillan* [1995] processed VLBI data down to 5° with this model and obtained the best performance with a 7° elevation angle cutoff. We also chose 7° as the elevation angle cutoff to be used with this model. At 7° elevation, a gradient with a magnitude of 1 mm corresponds to slant path delay of 67 mm.

3. Estimation Strategies and Experiment Setup

Many different approaches have been used to estimate the troposphere delay from GPS data. They usually differ in the choices of the temporal model for the delay and the elevation angle cutoff. The variety of temporal models commonly used range from a 2-hour piecewise constant model to a random walk model with updates every 5 min. Elevation angle cutoff values are typically 20° or 15°.

We experimented with a number of estimation strategies to evaluate the performance of the gradient model. All can be viewed as variants of the strategy currently employed at JPL for routine, precise positioning of ground sites (see below). All the experiments are carried out using the technique of point positioning. This powerful technique allows for rapid determination of a site's position, clock and troposphere delay parameters using previously determined GPS orbits and clocks [*Zumberge et al.*, 1997]. The dependence of the GPS orbits and clocks on the particular troposphere model used in the "global solution" is weak due to the large number ($\sim$ 40) of sites used in the global solution. We have verified that GPS orbits and clocks are insensitive to variations in receiver elevation angle cutoff but they do improve somewhat (see below) when gradients are modeled. For the fixed GPS orbits and clocks we used the JPL precise solutions for the International GPS Service for Geodynamics (IGS) [*Zumberge et al.*, 1995]. These orbits and clocks solutions were produced without the gradient model.

We designed a series of experiments to assess the impact of the troposphere gradient model on the estimate of a site's position. In the absence of truth values we evaluate the various estimation strategies mainly through their internal consistency, namely, the day-to-day repeatability of the site positions. In isolated cases we were able to compare GPS-based estimates of troposphere delay to those derived from a collocated WVR, thus establishing a more direct evaluation of performance through a comparison with an independent technique.

Table 3. Average Absolute Coordinate Biases Between Pairs of Estimation Strategies for the 37 Sites With More Than 2% of all Measurements Between 10° and 7°

Strategies	Radial	Latitude	Longitude
Current JPL and nominal homogeneous	1.22	0.08	0.08
Current JPL and tuned inhomogeneous	0.99	0.12	0.10
Nominal homogeneous and tuned inhomogeneous	0.30	0.19	0.11
Current JPL and tuned 15°	0.30	0.14	0.13

Units in centimeters.

Table 4. Mean and Scatter Around the Mean (Sigma) of WVR Minus GPS Estimates of ZWD for GOL3 and ONSA

Strategy	GOL3		ONSA	
	Mean	Sigma	Mean	Sigma
Current JPL	0.382	0.545	-0.396	0.711
Nominal homogeneous	0.122	0.535	-0.041	0.550
Tuned inhomogeneous	0.095	0.488	-0.041	0.507

The GOL3 comparison includes 3797 data points. The ONSA comparison includes 935 data points. Units in centimeters.

The data set for our experiments comprises measurements from all IGS sites ($\sim$ 150) available during October to December, 1996. This resulted in about 13,500 site days. In the experiments described below we point-positioned a subset of all of the IGS sites during this period to form a statistically significant comparison between the various strategies.

The estimation strategies we experimented with are described below. Each is assigned a name that will be used later in the text to refer to that strategy. Table 1 summarizes the differences between the various estimation strategies employed in our experiments.

3.1. Current JPL Strategy

The current JPL routine processing strategy for precise point positioning of a given site uses 24 hours of data from the ground receiver centered around noon UTC. Phase measurements are selected once every 5 min and are also used to smooth the pseudorange measurements to the 5-min mark. An elevation angle cutoff value of 15° is used, and the troposphere mapping function is that of *Lanyi* [1984]. The site's position vector is estimated daily as a constant. The receiver's clock is modeled as a white noise process with updates at every measurement epoch, and the wet zenith delay D_{wz} is modeled as random walk with unconstrained a priori and a random walk sigma of 10.2 mm/$\sqrt{\text{h}}$. A post fit residual window filters out all phase measurements with post-fit error larger than 5 cm [*Zumberge et al.*, 1995]. (In our experiments with the current JPL strategy we replaced Lanyi's mapping function with that of *Niell* [1996]. The impact of this switch is negligible.) (Please see note in the discussion section regarding recent changes to JPL's estimation strategy.)

3.2. Nominal Homogeneous Strategy

This strategy is identical to the current JPL strategy but with elevation angle cutoff reduced to 7° and random walk sigma for D_{wz} reduced to 3 mm/$\sqrt{\text{h}}$. This was found to be consistently superior to the current JPL strategy [*Bar-Sever*, 1996; *Bar-Sever and Kroger*, 1996].

3.3. Nominal Inhomogeneous Strategy

This was our first attempt at estimating the troposphere gradients. This strategy is identical to the nominal homogeneous strategy, but in addition to the wet zenith delay D_{wz}, we solve for the two components of the gradient vector G_N and G_E modeled as random walk processes, with unconstrained a priori and a random walk sigma of 0.6 mm/$\sqrt{\text{h}}$.

3.4. Constant Gradient Strategy

This strategy estimates a single daily gradient. It is identical to the nominal inhomogeneous strategy, except that the gradient is modeled as constant over a day. We included this strategy as an alternative for those who do not use stochastic models.

3.5. Tuned Inhomogeneous Strategy

This strategy is identical to the nominal inhomogeneous strategy, but the random walk sigma for the gradient parameters is reduced to 0.3 mm/$\sqrt{\text{h}}$ and the post fit residual window is reduced to 2.5 cm. This was made in an effort to improve the performance of the gradient model.

3.6. Tuned 15° Strategy

This strategy is identical to the tuned inhomogeneous strategy except that the elevation angle cutoff was raised to 15°. This strategy was used in order to check if the benefits of the tuned inhomogeneous strategy persist at a higher elevation angle cutoff.

4. Results From the Point Positioning Experiments

It is evident from (2) that the effect of horizontal gradients diminishes quickly as the elevation angle increases [see also *Gardner*, 1977; *Davis et al.*, 1993].

Table 5. Formal Errors in the GPS- and WVR-Based Estimates of the Troposphere Gradients

Gradient Component	GPS		WVR	
	Mean	Sigma	Mean	Sigma
G_N	0.033	0.008	0.007	0.004
G_E	0.030	0.009	0.007	0.004

Units in centimeters.

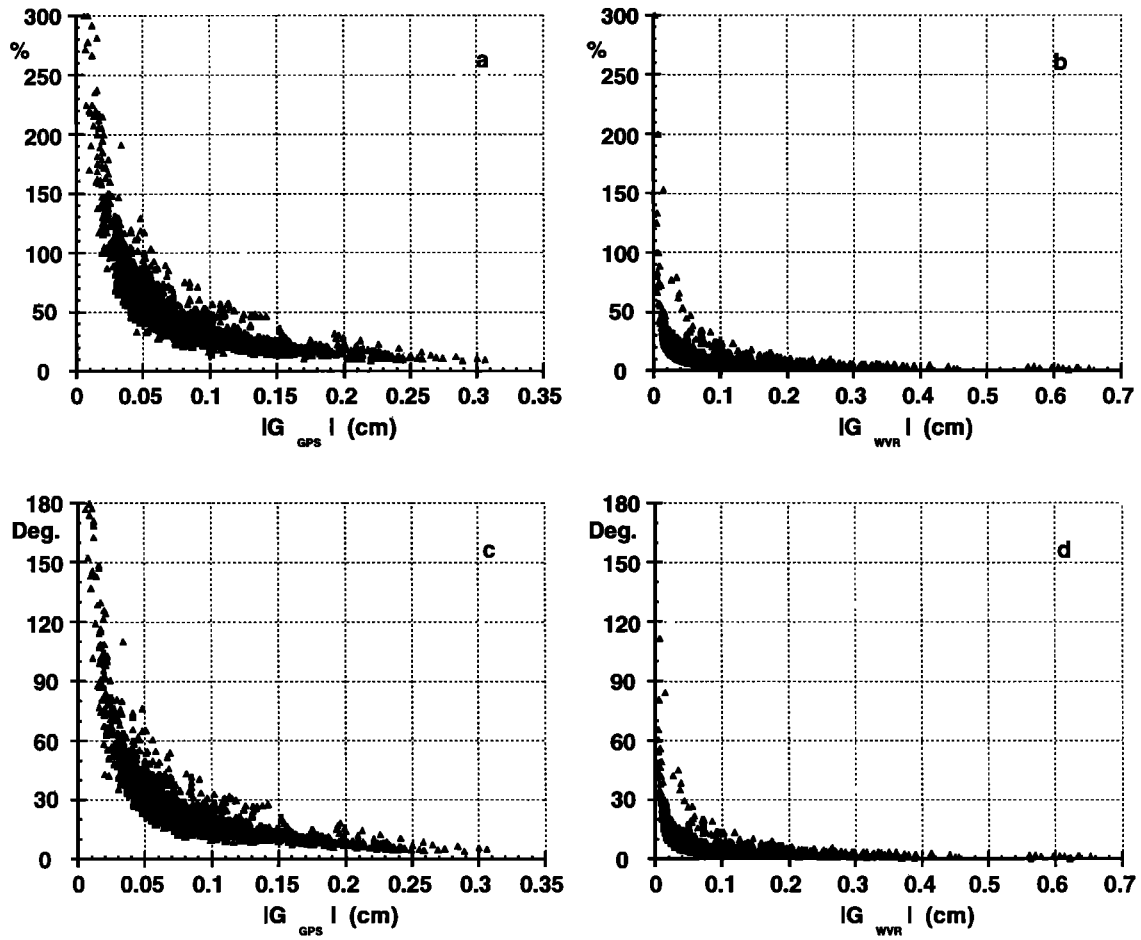

Figure 4. Formal errors in the magnitudes and azimuths of the GPS- and WVR-based gradients. (a) Formal errors in the magnitudes of the GPS-based gradients as percentage of the magnitudes. (b) Same as in Figure 4a but for the WVR. (c) Formal errors in the azimuths of the GPS-based gradients. (d) Same as in Figure 4c but for the WVR.

Therefore to sense the gradients it might be necessary to include low elevation angle observations. At the same time, reducing the elevation angle cutoff too much may result in increased errors from multipath and troposphere mapping function. We chose an elevation angle cutoff of 7° as a reasonable compromise. This choice is supported by *Bar-Sever* [1996] who reports superior agreement in wet zenith delay estimates between a collocated WVR and a GPS receiver, using this cutoff value, and by *MacMillan and Ma* [1994] who report improved VLBI baseline length repeatabilities using this cutoff value.

We began with a massive experiment intended to isolate the impact of the gradient model on point positioning by comparing the performance of the nominal inhomogeneous strategy and the nominal homogeneous strategy. In this experiment we independently point-positioned twice all the available IGS sites during October - December 1996 for each strategy. For each site we computed the mean position and velocity vectors, weighted by the formal errors, and the weighted daily repeatabilities in the radial, longitude and latitude components of the position vector around these means. At this point the only quality control measure applied was the rejection of one site, CMBB (part of the BARD network in northern California), because an 8-cm radial repeatability indicated a serious problem with the receiver/site. The mean improvement in three-dimensional position repeatabilities (3-D) due to the gradient model was a modest 1.6%, and many sites seem to be affected negatively by the gradient model. Figure 1 reveals a correlation between the performance of the nominal inhomogeneous model and the percentage of low elevation angle observations. Similar behavior is exhibited by the formal errors of the gradient vector and the position vector. Figure 2 shows the formal errors for the gradient (defined as the RMS of the formal errors for G_N and G_E) as a function of the percentage of measurements between 7° and 15°. Figure 1 also reveals that, on average, the percentage of low-elevation observations at an IGS site is very low; only 7% of all measurements are taken between 7° and 15°, and only 1.2% between 7° and 10° (compared to theoretical 14% and 5%, respectively, assuming all in view tracking and a uniform distribution of the GPS satellites in the local sky).

The preceding results clearly demonstrate the need for a sufficient number of low elevation angle measure-

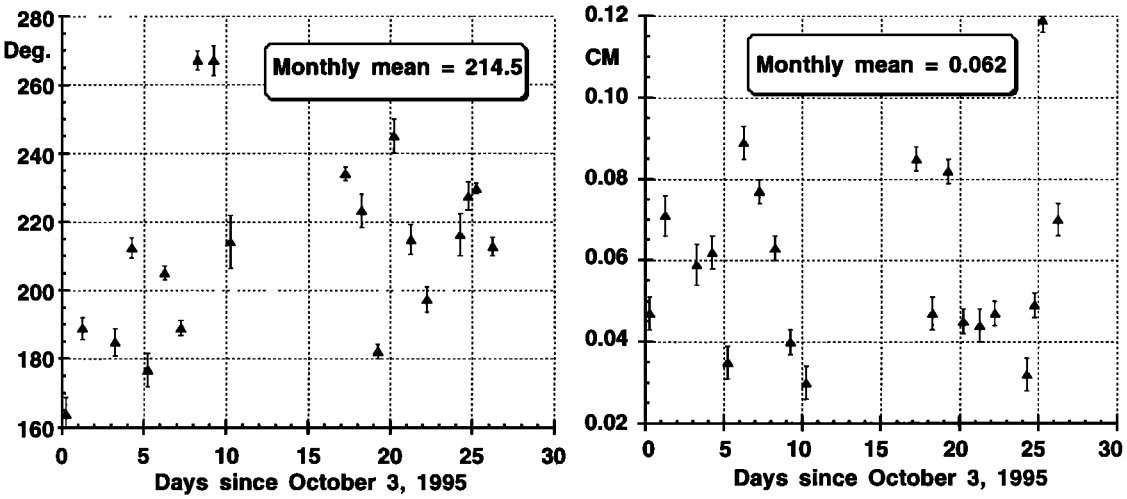

Figure 5. The observed hydrostatic gradients derived as the vector biases between the GPS-based gradients and the WVR-based gradient for each 12-hour segment: (left) azimuth, and (right) magnitude.

ments to realize significant improvement with the gradient model. Subsequent experiments were carried out therefore on a subset of stations that meet a minimal criterion for the percentage of low elevation angle measurements. Based on Figure 1, that criterion was chosen to be 2% of the total number of measurement taken between 7° and 10° elevation. Figure 1 shows that most sites satisfying this criterion display improvement in position repeatability. 37 out of the 150 IGS sites that participated in our experiment satisfied this criterion, on average, during October - December 1996.

We also attempted to improve the performance of the gradient model by tuning the estimation strategy on a small number of sites. The two tuning parameters were the random walk sigma for the gradient parameters and the size of the rejection window for postfit phase residuals. Figure 3 depicts the tuning process for one site, AOA1 (in southern California), that performed rather poorly with the nominal inhomogeneous strategy. The results suggested that our nominal inhomogeneous strategy was suboptimal. Halving the size of the postfit phase window and of the random walk sigma from their nominal value gave superior results. The reduction in postfit window size is probably an artifact of the increase in the number of degrees of freedom due to the gradient parameters.

Next, we tested all six strategies in Table 1 on the 37 sites that satisfied the minimum criterion for low-elevation measurements. For each estimation strategy and for each site we computed the repeatability in the daily position estimates. Table 2 summarizes the mean improvement in position repeatability for each strategy relative to the repeatability obtained with the current JPL strategy. The tuned inhomogeneous strategy proved to be far superior to the five other tested strategies for this data set in all components of the position vector. The mean improvement in 3-D position repeatability was 18.5% relative to the current JPL strategy. Only two sites, STJO (St. John, Canada) and YAR1 (Yaragadee, Australia), experienced small degradation in 3-D position repeatability due to the tuned inhomogeneous strategy as compared to the current JPL strat-

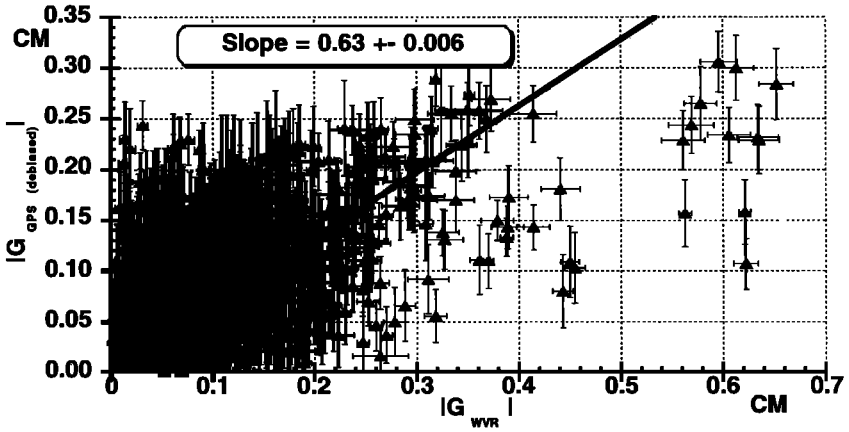

Figure 6. Magnitude of the (debiased) GPS-based gradient vector plotted against the magnitude of the WVR-based estimates of the gradient vector. The slope of line that fits the data in a weighted least squares sense is shown in the inset box together with its standard deviation.

Table 6. Statistics of the Difference Between GPS and WVR Estimates of the Tropospheric Gradients

Subset	No. of Points	Mean Relative Magnitude of difference, %	Mean Azimuth Diference, deg.	Linear Correlation in Magnitude	Slope of Linear fit for Magnitude
All points	1374	63	29	0.56	0.63
$\|G_{WVR}\| > 0.1$ cm	490	58	19	0.50	0.56
$\|G_{WVR}\| > 0.2$ cm	135	55	10	0.38	0.49
$\|G_{WVR}\| > 0.3$ cm	46	60	8	0.21	0.43
$\|G_{WVR}\| < 0.3$ cm	1328	66	33	0.49	0.75
$\|G_{WVR}\| < 0.2$ cm	1237	75	38	0.37	0.84
$\|G_{WVR}\| < 0.1$ cm	878	96	46	0.22	1.10

Four statistical parameters are computed for seven subsets of the complete data set of 1374 points. The statistical parameters are (1) mean relative magnitude of difference, that is, the weighted mean of $100|G_{WVR} - G_{GPS}|/|G_{WVR}|$; (2) mean azimuth difference, that is, the weighted mean of $|\angle G_{WVR} - \angle G_{GPS}|$; (3) the weighted linear correlation (also known as Pearson's r) between $|G_{WVR}|$ and $|G_{GPS}|$; (4) the slope of the line with zero intercept that best fit the set of pairs $(|G_{WVR}|, |G_{GPS}|)$ in a weighted least squares sense.

egy. The relative improvement for each of the participating sites and for each strategy is given in Table 7.

The repeatability of the radial component of the position vector improves, on average, when lowering the elevation angle, regardless of the details of the gradient model, in agreement with a number of other studies of GPS [*Bar-Sever and Kroger,* 1996] and VLBI [*MacMillan and Ma,* 1994]. The presence of the gradient model is seen to improve the radial repeatability even further, and the best repeatabilities are obtained with the tuned inhomogeneous strategy, with average radial repeatability improvement of 19.5%. Only four sites, ONSA (Onsala, Sweden), REYK (Reykjavik, Iceland), STJO, and YAR1, experienced degradation in the radial position repeatabilities due to the tuned inhomogeneous strategy.

The horizontal component of the estimated position vector behaves markedly differently than the radial component. Table 2 demonstrates that a reduction in elevation angle cutoff value without the additional estimation of a troposphere gradient will tend to degrade the repeatability of the horizontal components. The best results are, again, obtained with the tuned inhomogeneous strategy. It is noteworthy that the repeatability of the horizontal component of the position vector using the tuned 15° strategy was superior to all other strategies, except the tuned inhomogeneous strategy.

Bar-Sever and Kroger [1996] have shown that the choice of elevation angle cutoff value affects the mean of the radial component of the estimated position vector as well as its scatter. Indeed, Table 3 reveals that significant radial biases are associated with the change of elevation angle cutoff. The presence of the gradient model tends to reduce the bias associated with elevation angle cutoff by about 25%. The impact of the gradient model on the biases in the horizontal coordinates is larger than that of the elevation angle cutoff value, but both are very small. There are too few southern hemisphere sites in our experiments to form a meaningful distinction between their response to the various strategies and the response of the northern hemisphere sites.

5. Comparison Between GPS and WVR Wet Zenith Delay Estimates

The next set of experiments were designed to gauge the impact of the gradient model on the GPS solution through an independent evaluation of an important GPS product, namely, the zenith wet delay (ZWD). Such evaluations have been carried out extensively by many researchers, as an effort to validate the GPS-based estimates for meteorological applications. The WVR has been the primary tool in these evaluations due to its high level of precision and because it is considered a more established technology for the retrieval of ZWD [*Bar-Sever,* 1996; *Businger et al.,* 1996; *Duan et al.,* 1996; *Runge et al.,* 1995; *Wolfe and Gutman,* 1994]. We were able to carry out a ZWD comparison between a GPS receiver and a WVR at two sites, GOL3 (Goldstone, California) and ONSA (Onsala, Sweden). See the next section for more information about this WVR. The comparison at GOL3 spanned 30 days in July 1996, and the comparison at ONSA spanned 28 days in October 1995. The GOL3 receiver had a moderate number of low-elevation observations during the experiment: 1.2% between 7° and 10°, and 7.7% between 7° and 15°. The ONSA receiver is consistently better in that regard (see next section). For each of these sites we had available precise measurements of surface pressure, which enabled us to extract the ZWD from the TZD. Each site was point-positioned daily using three estimation strategies: the current JPL strategy, the nominal homogeneous strategy and the tuned inhomogeneous strategy. The results of the comparisons are summarized in Table 4. As Table 4 indicates, a reduction in scatter around the mean is associated with the lowering of elevation angle cutoff for GPS observations and is a well-known phenomenon [*Bar-Sever and Kroger,* 1996; *Runge et al.,* 1995]. Most importantly, Table 4 links the gradient model to a significant additional reduction in the scatter around the mean of the WVR-GPS differences. The tuned inhomogeneous strategy is shown to yield the best agreement with the WVR for both sites.

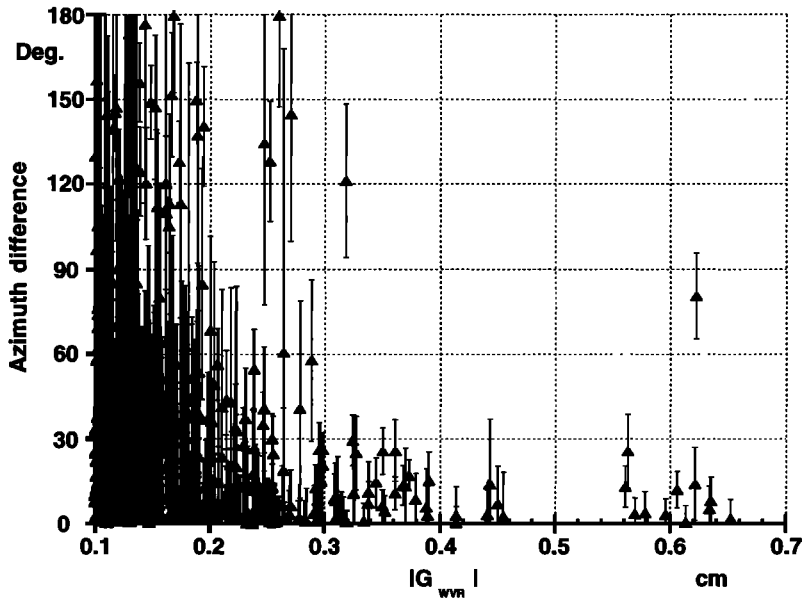

Figure 7. Differences in the azimuths between the GPS- and the WVR-based estimates of the gradient vectors as a function of the WVR-based magnitude of the vector.

6. Direct Evaluation of the Gradient Estimates

While it is clear that employing the troposphere gradient model as part of the tuned inhomogeneous strategy improves the quality of the GPS solution, the reasons for this improvement are uncertain. The simplest explanation is that the gradient model was able to absorb actual tropospheric inhomogeneities. This must be verified before the estimated gradients can be used in meteorological applications. In this section we present some evidence that strongly supports this explanation. We do so by comparing GPS-based estimates of troposphere gradients to those based on a collocated WVR. Since water vapor varies on small spatial scales, the WVR and the GPS receiver must be in close proximity. To serve our purposes, the GPS has to track low-elevation angles well, and the WVR has to observe a broad range of azimuth and elevation angles. The WVR retrieval algorithm must be well calibrated. Opportunities to compare GPS and WVR measurements are very limited as a result of these stringent requirements. Fortunately, such opportunity exists at Onsala, Sweden, where a WVR is located less than 10 m away from the IGS receiver, ONSA. This GPS receiver is one of best in terms of tracking low-elevation observations (see Table 7).

Zenith equivalent of WVR-based line-of-site estimates of wet delay during October 1995 were kindly supplied by Per Jarlemark from the Onsala Space Observatory. They consist of approximately 6500 measurements per day at 14 uniformly spaced azimuth angles and at seven elevation angles, spanning the range from 21.4° to 90°. Altogether, there are 37 distinct azimuth-elevation pairs. During October 1995, the average fraction of measurements from the ONSA GPS receiver taken between 7° and 10° was 5.8% and those taken between 7° and 15° was 15.3%.

We point-positioned the ONSA receiver during each day in October 1995 using our tuned inhomogeneous strategy. This resulted in a time series of gradient components, G_N and G_E, spanning the whole month of October, with an interval of 5 min. Since the WVR does not produce gradient estimates directly, they were derived from the line-of-sight observations as follows. We linearly interpolated all the measurements to a common time series such that the interpolation step size was always less than 5 min and such that at each interpolated time point all the 37 distinct azimuth-elevation measurements were available. This resulted in a data set consisting of 2198 time points. At each time point we have 37 measurements of wet delay at different azimuth and elevation pairs. For each time point we used the 37 measurements as left-hand side observations in (2) and estimated the gradient vector together with the ZWD in a least squares formalism. This process is analogous to the GPS solution process where several distinct line-of-sight observations are combined in time and space to form the estimate of the gradient. To compare the WVR-based estimates with the GPS-based estimates, we interpolated the GPS-based estimates to the WVR time series. Since GPS estimates are given every 5 min, the interpolation step size is always less than 5 min. The WVR-based estimates of ZWD that were used in the comparison with the GPS-based estimates, above, were derived by this process. The excellent agreement with the GPS-based estimates of ZWD, reported in Table 4, offers some validation for this approach.

The formal errors of the GPS- and WVR-based gradient estimates are summarized in Table 5 and the cor-

responding uncertainties in the magnitude and azimuth of the vectors are illustrated in Figure 4. The WVR-based estimates are formally more accurate than the GPS-based estimates by a factor of 5.

At this point the GPS-based gradients are not likely to compare well with the WVR-based gradients. This is because the GPS-based gradients include a hydrostatic component that is absent from the WVR data. Because the hydrostatic gradient varies, typically, on a much longer timescale than the wet gradient [*Davis et al.*, 1993; *MacMillan*, 1995], we might be able to remove it using independent observations, from objective analysis, or from a local climatology of the hydrostatic gradient. To simulate this approach, we assumed that the hydrostatic gradient changes on a 12-hour scale. We partitioned the data set into 12-hour segments, centered on local noon and midnight, and we debiased the GPS-based gradient estimates at each segment with respect to the WVR-based gradients. That is, the mean difference between the GPS-based gradient and the WVR-based gradient during each segment was removed. This also enabled us to include all the segments in one data set. We further restricted our data set to those 12-hour segments that contain measurements at least every 15 min. This final data set contained twenty 12-hour segments and 1374 points. The hydrostatic gradients extracted in this way are presented in Figure 5. A prevailing hydrostatic gradient roughly in the north-south direction and 0.06 cm in magnitude is observed. The month- long mean in the GPS total delay gradient had a magnitude of 0.03 cm and azimuth of 194° (that translates to a delay of 9.8 mm at 10° elevation and agrees quit well with the 3 years mean total gradient of 10.2 mm and 164° azimuth estimated by *Chen and Herring* [1997] using the Onsala VLBI.) The monthly mean wet gradient, as observed by the WVR, has a similar magnitude, but an azimuth of 45°, approximately. The similarity in magnitude of the mean hydrostatic gradient and wet gradient hampers our ability to separate these components based on long-term averages and highlights the need to fold in independent observations of the hydrostatic gradient.

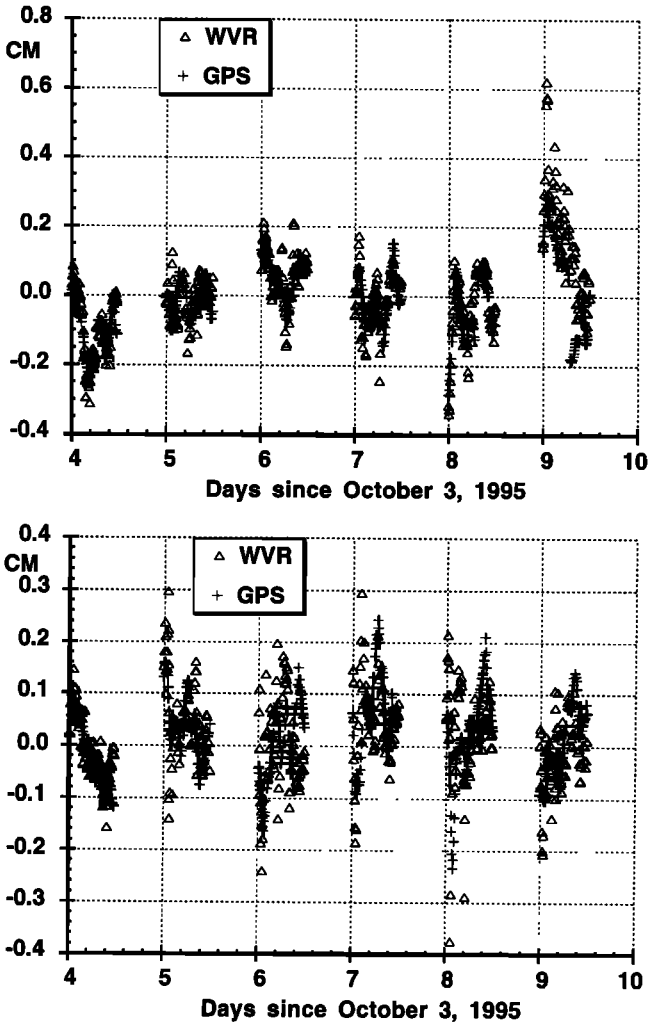

Figure 8. GPS- and WVR-based estimates of (top) G_N and (bottom) G_E for six 12-hour segments during October 1995. Note that the bias between the GPS and the WVR estimates for each segment was removed. Only six segments are shown for clarity. Other segments are similar. The absence of every other 12-hour segment is a result of the requirement for having a WVR data point at least every 15 min. Most 12-hour segments centered on noon did not fulfill this requirement for unknown reasons. The midnight-centered segments include the day's boundary and can display therefore some discontinuity in the estimates. Such discontinuities can be observed with G_N in the fifth and sixth segments.

Figure 6 illustrates the correlation between the GPS-based wet gradient estimates and the WVR- based estimates in terms of the magnitude of the vectors. The linear correlation between the GPS- based magnitude and the WVR-based magnitude is 0.56, which is significant at the 100% level (i.e., very unlikely to be a random occurrence). The slope of the linear fit, displayed in Figure 5, tends to get closer to 1 when large gradients are excluded from the fit, but that causes the linear correlation to degrade (Table 6). Table 6 reveals that the GPS-based gradients systematically differ from the WVR-based gradients by about 60%. For large gradients, this discrepancy is due to the GPS-based magnitudes being uniformly smaller than the WVR-based magnitudes. For weaker gradients, the discrepancy appears to be noisy. In contrast, the two technologies display a remarkable agreement in the azimuth of the gradient vector, with better than 10° agreement for strong gradients (larger than 0.2 cm in magnitude). The agreement in azimuth improves as the gradient magnitudes get larger as is illustrated in Figure 7. Finally, a sample of wet gradient estimates from each technology is depicted in Figure 8, showing good correlation between the two solutions.

7. Discussion

In the first part of this paper we demonstrated that utilization of the troposphere gradient model with a proper estimation strategy leads to improvements in

Table 7. Point-Positioning Statistics for the 37 Sites on Which Five Estimation Strategies were Tested

Site	%15	%10	%rad	%lat	%lon	%2-D	%3-D	%chi	rad	lat	lon
AOA1[a]	...	...	...	...	...	...	...	...	1.22	0.32	0.48
AOA1[b]	8.71	2.21	28.93	-2.11	-4.88	-4.02	21.89	-30.81	0.87	0.33	0.50
AOA1[c]	8.71	2.21	35.32	-3.32	-6.47	-5.49	26.69	-8.06	0.79	0.33	0.51
AOA1[d]	8.81	2.27	22.28	-3.26	-1.74	-2.22	17.28	11.71	0.95	0.33	0.49
AOA1[e]	0.00	0.00	21.51	4.69	17.60	13.33	20.04	55.38	0.96	0.30	0.40
AOA1[f]	8.04	1.88	40.99	15.55	20.73	19.08	36.44	42.78	0.72	0.27	0.38
ASC1[a]	...	...	...	...	...	...	...	...	1.24	0.51	1.06
ASC1[b]	13.11	3.11	0.23	-4.81	-1.30	-1.97	-0.83	-39.69	1.24	0.53	1.07
ASC1[c]	13.11	3.11	2.64	-4.51	0.88	-0.21	1.29	-7.39	1.21	0.53	1.05
ASC1[d]	13.12	3.11	8.95	-4.40	1.04	-0.01	4.58	26.40	1.13	0.53	1.05
ASC1[e]	0.00	0.00	-6.59	-3.89	2.39	1.11	-3.03	46.00	1.32	0.53	1.03
ASC1[f]	12.73	3.02	6.80	-3.25	4.14	2.70	4.83	19.28	1.16	0.53	1.02
AUCK[a]	...	...	...	...	...	...	...	...	0.96	0.51	0.69
AUCK[b]	10.77	2.62	-3.44	-5.89	0.38	-1.92	-2.77	-45.41	0.99	0.54	0.69
AUCK[c]	10.77	2.62	8.17	6.50	3.41	4.49	6.50	-1.47	0.88	0.48	0.67
AUCK[d]	10.90	2.70	13.02	7.64	3.54	5.00	9.37	24.96	0.84	0.47	0.67
AUCK[e]	0.00	0.00	7.22	10.60	9.32	9.77	8.35	53.46	0.88	0.46	0.63
AUCK[f]	10.53	2.61	14.12	10.95	6.85	8.31	11.50	22.79	0.82	0.45	0.64
BOR1[a]	...	...	...	...	...	...	...	...	0.70	0.45	0.58
BOR1[b]	6.75	2.06	10.56	-3.90	0.40	-1.22	4.20	-23.16	0.63	0.47	0.58
BOR1[c]	6.75	2.06	8.50	12.26	6.39	8.46	8.48	20.84	0.64	0.39	0.54
BOR1[d]	6.78	2.08	9.55	12.02	6.48	8.49	9.00	40.09	0.63	0.40	0.54
BOR1[e]	0.00	0.00	5.53	23.69	30.32	27.86	16.64	67.08	0.66	0.34	0.40
BOR1[f]	6.65	2.04	16.60	19.15	33.10	27.62	22.18	51.86	0.58	0.36	0.39
CAGL[a]	...	...	...	...	...	...	...	...	0.79	0.41	0.51
CAGL[b]	9.33	3.03	14.67	-13.62	-0.20	-5.77	5.82	-55.09	0.67	0.47	0.51
CAGL[c]	9.33	3.03	5.66	5.75	2.02	3.46	4.77	-4.89	0.75	0.39	0.50
CAGL[d]	9.41	3.09	17.79	7.81	0.81	3.54	11.72	25.92	0.65	0.38	0.51
CAGL[e]	0.00	0.00	10.91	11.11	14.17	12.96	11.73	56.26	0.70	0.36	0.44
CAGL[f]	8.98	2.94	12.54	11.74	4.64	7.41	10.42	22.74	0.69	0.36	0.49
CIT1[a]	...	...	...	...	...	...	...	...	1.10	0.35	0.48
CIT1[b]	9.17	2.16	13.97	-6.96	-1.82	-3.61	9.72	-50.04	0.95	0.37	0.49
CIT1[c]	9.17	2.16	20.73	-0.46	-1.73	-1.30	15.67	-9.31	0.87	0.35	0.49
CIT1[d]	9.20	2.17	19.12	-2.10	-0.46	-1.02	14.18	17.52	0.89	0.36	0.48
CIT1[e]	0.00	0.00	34.17	24.78	23.48	23.92	31.91	68.14	0.72	0.26	0.37
CIT1[f]	9.12	2.15	34.60	23.71	22.12	22.66	31.73	46.19	0.72	0.27	0.37
COCO[a]	...	...	...	...	...	...	...	...	1.91	0.74	0.86
COCO[b]	13.97	3.85	12.41	-4.30	-6.56	-5.60	7.38	-42.72	1.67	0.77	0.92
COCO[c]	13.97	3.85	20.75	9.27	6.04	7.37	17.15	18.37	1.51	0.67	0.81
COCO[d]	14.86	4.42	12.95	10.96	-2.21	3.18	10.30	24.61	1.66	0.66	0.88
COCO[e]	0.00	0.00	4.68	-8.32	5.25	-0.62	3.31	47.55	1.82	0.80	0.81
COCO[f]	13.33	3.56	22.33	3.17	10.02	7.04	18.07	30.40	1.48	0.72	0.77
FARB[a]	...	...	...	...	...	...	...	...	1.25	0.35	0.53
FARB[b]	15.71	5.68	11.48	-23.15	-11.59	-15.25	5.25	-110.53	0.31	0.65	0.00
FARB[c]	15.71	5.68	24.29	-0.79	3.08	1.87	19.21	-19.48	0.95	0.35	0.51
FARB[d]	15.91	5.81	24.67	-2.62	3.14	1.34	19.23	6.19	0.94	0.36	0.51
FARB[e]	0.00	0.00	19.53	6.06	12.26	10.31	17.56	56.63	1.01	0.33	0.47
FARB[f]	15.70	5.74	38.95	23.21	24.14	23.86	35.49	38.82	0.76	0.27	0.40
FORT[a]	...	...	...	...	...	...	...	...	1.36	0.52	0.83
FORT[b]	14.16	4.19	23.25	-9.35	12.57	5.81	16.86	-52.48	1.04	0.57	0.73
FORT[c]	14.16	4.19	25.07	5.87	7.70	7.17	18.85	23.30	1.02	0.49	0.77
FORT[d]	14.40	4.30	22.75	3.28	4.16	3.91	15.81	42.73	1.05	0.50	0.80
FORT[e]	0.00	0.00	9.38	2.93	-0.46	0.51	6.42	61.89	1.23	0.50	0.83
FORT[f]	13.42	3.99	27.72	4.92	7.00	6.40	19.77	42.32	0.98	0.49	0.77
GRAS[a]	...	...	...	...	...	...	...	...	0.92	0.37	0.42
GRAS[b]	12.10	3.33	20.42	-6.47	-5.84	-6.11	12.40	-48.67	0.73	0.39	0.44
GRAS[c]	12.10	3.33	23.47	0.59	-0.89	-0.25	16.60	-15.74	0.70	0.37	0.42
GRAS[d]	12.20	3.41	26.55	0.95	-6.97	-3.63	17.24	10.97	0.68	0.37	0.45
GRAS[e]	0.00	0.00	12.77	3.30	6.51	5.11	10.69	48.01	0.80	0.36	0.39
GRAS[f]	10.98	2.98	25.57	3.90	7.94	6.18	19.83	12.30	0.68	0.36	0.39

Table 7. (continued)

Site	%15	%10	%rad	%lat	%lon	%2-D	%3-D	%chi	rad	lat	lon
HBRK[a]	...	...	...	...	...	...	...	...	0.85	0.31	0.60
HBRK[b]	11.55	2.27	-3.36	-5.84	8.55	5.33	-0.06	-49.26	0.88	0.33	0.55
HBRK[c]	11.55	2.27	-0.89	7.55	24.47	20.78	7.33	-0.08	0.86	0.29	0.45
HBRK[d]	11.64	2.32	-1.65	10.20	13.59	12.86	3.75	16.11	0.86	0.28	0.52
HBRK[e]	0.00	0.00	-0.47	18.46	33.19	29.98	10.68	61.99	0.85	0.25	0.40
HBRK[f]	11.09	2.17	9.34	25.57	34.00	32.14	17.48	39.95	0.77	0.23	0.40
HKLO[a]	...	...	...	...	...	...	...	...	0.99	0.31	0.70
HKLO[b]	11.95	2.01	15.07	-8.02	3.28	1.31	9.67	-46.31	0.84	0.33	0.68
HKLO[c]	11.95	2.01	26.12	2.21	11.24	9.72	19.35	-2.73	0.73	0.30	0.62
HKLO[d]	12.07	2.07	12.50	0.54	17.19	14.21	13.13	17.99	0.87	0.31	0.58
HKLO[e]	0.00	0.00	3.63	26.06	22.00	7.96	51.78	37.63	0.95	0.23	0.55
HKLO[f]	11.32	1.98	18.91	19.74	30.58	28.67	22.43	37.63	0.80	0.25	0.49
HOPB[a]	...	...	...	...	...	...	...	...	1.25	0.37	0.59
HOPB[b]	16.54	6.10	13.16	-17.67	-2.24	-6.95	8.00	-103.86	0.32	0.69	0.00
HOPB[c]	16.54	6.10	17.52	-4.33	3.72	1.33	13.58	-37.76	1.03	0.39	0.57
HOPB[d]	16.71	6.23	19.40	1.28	7.31	5.52	15.91	1.69	1.01	0.37	0.55
HOPB[e]	0.00	0.00	13.11	4.49	19.56	14.93	13.52	54.35	1.09	0.35	0.47
HOPB[f]	16.45	6.12	29.22	12.81	20.20	17.99	26.40	19.46	0.88	0.32	0.47
KELY[a]	...	...	...	...	...	...	...	...	0.99	0.34	0.57
KELY[b]	10.41	2.62	21.47	-15.30	-4.98	-7.80	11.35	-64.15	0.78	0.39	0.60
KELY[c]	10.41	2.62	17.42	1.37	9.28	7.18	14.17	-25.40	0.82	0.34	0.52
KELY[d]	10.44	2.62	18.09	2.95	9.46	7.70	14.73	11.66	0.81	0.33	0.52
KELY[e]	0.00	0.00	14.47	5.43	15.08	12.49	13.86	42.81	0.85	0.32	0.48
KELY[f]	10.26	2.62	21.79	12.91	19.96	18.04	20.61	18.87	0.77	0.30	0.46
KWJ1[a]	...	...	...	...	...	...	...	...	2.02	0.59	1.07
KWJ1[b]	13.54	3.37	20.86	-10.20	-3.03	-4.74	13.25	-41.13	1.60	0.65	1.10
KWJ1[c]	13.54	3.37	24.53	22.93	0.32	4.75	18.75	23.77	1.52	0.45	1.07
KWJ1[d]	14.01	3.58	27.81	22.53	-0.97	3.97	20.71	47.00	1.46	0.46	1.08
KWJ1[e]	0.00	0.00	15.65	22.22	11.50	13.70	15.12	63.43	1.70	0.46	0.95
KWJ1[f]	12.11	3.14	30.83	28.93	4.96	9.95	24.66	51.38	1.40	0.42	1.02
LMNO[a]	...	...	...	...	...	...	...	...	0.87	0.35	0.61
LMNO[b]	12.62	2.53	10.32	-7.48	7.34	3.49	7.55	-45.12	0.78	0.38	0.57
LMNO[c]	12.62	2.53	14.21	-2.02	15.25	10.84	12.80	-8.42	0.75	0.36	0.52
LMNO[d]	12.72	2.58	15.67	1.43	16.89	12.84	14.54	18.08	0.73	0.34	0.51
LMNO[e]	0.00	0.00	2.42	4.50	24.20	19.08	8.97	51.79	0.85	0.33	0.46
LMNO[f]	12.21	2.44	17.35	14.10	25.96	22.89	19.50	30.08	0.72	0.30	0.45
METS[a]	...	...	...	...	...	...	...	...	0.73	0.28	0.50
METS[b]	13.93	4.15	8.15	-6.70	9.57	5.46	7.12	-47.77	0.67	0.30	0.45
METS[c]	13.93	4.15	9.72	-0.49	22.11	16.42	12.27	-11.97	0.66	0.28	0.39
METS[d]	13.96	4.17	14.60	-0.91	-0.26	-0.42	8.63	2.09	0.62	0.28	0.50
METS[e]	0.00	0.00	1.36	-4.92	29.21	20.14	8.21	49.47	0.72	0.29	0.35
METS[f]	13.93	4.16	16.07	3.59	21.28	16.74	16.32	12.01	0.61	0.27	0.39
MOIN[a]	...	...	...	...	...	...	...	...	1.79	0.55	1.11
MOIN[b]	14.05	3.25	-0.73	-17.97	-2.80	-5.99	-2.46	-61.91	1.80	0.65	1.14
MOIN[c]	14.05	3.25	2.83	16.99	-5.37	-1.18	1.55	7.94	1.72	0.46	1.17
MOIN[d]	14.54	3.45	19.56	14.55	-1.27	1.67	13.38	39.34	1.44	0.47	1.12
MOIN[e]	0.00	0.00	11.13	15.26	2.64	5.09	9.19	56.82	1.59	0.47	1.08
MOIN[f]	13.48	3.17	12.08	25.34	10.04	12.87	12.33	46.23	1.57	0.41	1.00
OAT2[a]	...	...	...	...	...	...	...	...	1.07	0.41	0.53
OAT2[b]	11.13	3.37	5.95	-13.22	-9.11	-10.66	0.96	-84.33	1.01	0.46	0.58
OAT2[c]	11.13	3.37	11.58	1.56	-9.20	-5.27	6.84	-22.96	0.95	0.40	0.58
OAT2[d]	11.19	3.41	8.49	5.64	-3.07	0.09	6.03	12.97	0.98	0.39	0.55
OAT2[e]	0.00	0.00	20.20	24.54	18.43	20.68	20.32	66.11	0.85	0.31	0.43
OAT2[f]	10.93	3.34	24.14	18.86	21.68	20.61	23.13	34.73	0.81	0.33	0.42
OBER[a]	...	...	...	...	...	...	...	...	0.77	0.24	0.44
OBER[b]	11.77	3.62	17.51	-13.99	4.24	-0.26	11.90	-52.33	0.64	0.27	0.42
OBER[c]	11.77	3.62	24.81	4.13	9.31	8.13	19.32	-8.56	0.58	0.23	0.40
OBER[d]	11.80	3.63	12.48	4.25	-8.22	-5.47	6.83	2.00	0.67	0.23	0.48
OBER[e]	0.00	0.00	2.38	16.84	0.90	4.23	2.94	37.75	0.75	0.20	0.44
OBER[f]	11.60	3.60	16.71	14.24	8.12	9.50	14.52	13.50	0.64	0.21	0.40
ONSA[a]	...	...	...	...	...	...	...	...	0.64	0.32	0.41

Table 7. (continued)

Site	%15	%10	%rad	%lat	%lon	%2-D	%3-D	%chi	rad	lat	lon
ONSA[b]	14.89	5.70	-11.50	-10.70	-13.55	-12.45	-11.88	-84.94	0.71	0.35	0.47
ONSA[c]	14.89	5.70	-4.74	-2.17	-0.81	-1.34	-3.40	-35.24	0.67	0.33	0.41
ONSA[d]	14.93	5.73	-7.79	-1.74	-4.71	-3.57	-6.13	-6.02	0.69	0.33	0.43
ONSA[e]	0.00	0.00	9.76	0.40	8.49	5.27	7.94	49.25	0.58	0.32	0.38
ONSA[f]	14.49	5.55	-2.36	1.61	10.86	7.16	1.33	-2.41	0.66	0.31	0.37
PLTC[a]	...	...	...	...	...	...	...	...	0.89	0.30	0.48
PLTC[b]	12.67	3.16	10.05	-0.60	-1.42	-1.19	6.70	-46.71	0.80	0.30	0.49
PLTC[c]	12.67	3.16	12.22	-10.56	-2.10	-4.55	7.12	-31.10	0.78	0.33	0.49
PLTC[d]	12.75	3.17	11.47	-6.92	1.68	-0.82	7.79	-1.11	0.79	0.32	0.47
PLTC[e]	0.00	0.00	17.74	15.20	16.35	16.02	17.24	58.66	0.73	0.25	0.40
PLTC[f]	12.06	3.00	22.19	16.84	19.05	18.42	21.10	28.77	0.69	0.25	0.39
POL2[a]	...	...	...	...	...	...	...	...	0.70	0.54	0.73
POL2[b]	10.19	2.44	10.07	-2.41	3.25	1.19	4.39	-34.08	0.63	0.55	0.71
POL2[c]	10.19	2.44	14.07	-2.56	1.67	0.14	5.08	1.52	0.60	0.55	0.72
POL2[d]	10.20	2.45	9.11	0.79	-0.44	-0.00	3.28	23.08	0.64	0.54	0.73
POL2[e]	0.00	0.00	-0.90	0.17	1.63	1.11	0.36	48.57	0.71	0.54	0.72
POL2[f]	10.14	2.41	11.94	0.96	6.94	4.76	7.36	19.92	0.62	0.53	0.68
REYK[a]	...	...	...	...	...	...	...	...	0.84	0.30	0.47
REYK[b]	12.35	3.46	-5.66	-35.69	-2.45	-12.99	-7.92	-114.80	0.32	0.64	0.00
REYK[c]	12.35	3.46	-5.46	17.08	10.30	12.19	-0.47	-19.36	0.89	0.25	0.42
REYK[d]	12.38	3.49	-0.95	14.01	14.36	14.26	3.38	10.79	0.85	0.26	0.40
REYK[e]	0.00	0.00	7.05	13.40	14.44	14.14	9.13	51.45	0.78	0.26	0.40
REYK[f]	12.01	3.45	-2.64	19.18	22.66	21.65	4.03	8.02	0.86	0.24	0.36
SPK1[a]	...	...	...	...	...	...	...	...	1.25	0.33	0.58
SPK1[b]	9.73	2.45	23.32	1.29	-6.18	-4.44	16.41	-39.69	0.96	0.33	0.62
SPK1[c]	9.73	2.45	17.11	-1.47	-3.74	-3.20	12.23	-18.57	1.04	0.33	0.60
SPK1[d]	9.77	2.47	18.86	4.45	-8.44	-5.50	12.91	6.06	1.01	0.32	0.63
SPK1[e]	0.00	0.00	19.68	16.91	20.68	19.76	19.70	57.87	1.00	0.27	0.46
SPK1[f]	9.34	2.38	33.66	21.09	16.94	17.92	29.89	35.29	0.83	0.26	0.48
STJO[a]	...	...	...	...	...	...	...	...	0.87	0.37	0.58
STJO[b]	13.95	4.82	-28.95	-14.60	-3.93	-7.15	-20.96	-97.35	1.12	0.42	0.60
STJO[c]	13.95	4.82	-30.21	0.51	4.98	3.65	-18.22	-43.77	1.13	0.37	0.55
STJO[d]	14.06	4.90	-11.99	-1.58	8.60	5.51	-5.54	2.57	0.97	0.38	0.53
STJO[e]	0.00	0.00	3.21	1.26	17.74	12.61	6.75	51.95	0.84	0.37	0.48
STJO[f]	13.65	4.79	-10.36	11.97	18.09	16.26	-0.86	7.17	0.96	0.33	0.48
THU1[a]	...	...	...	...	...	...	...	...	0.93	0.27	0.32
THU1[b]	10.53	2.23	17.52	-13.59	-20.97	-17.92	10.63	-89.45	0.77	0.31	0.39
THU1[c]	10.53	2.23	26.51	-11.44	1.83	-3.96	20.61	-19.27	0.68	0.30	0.31
THU1[d]	10.57	2.25	27.60	-12.14	6.15	-1.94	21.89	4.22	0.67	0.30	0.30
THU1[e]	0.00	0.00	8.37	-5.04	10.09	3.44	7.53	42.90	0.85	0.28	0.29
THU1[f]	10.03	2.13	29.55	-8.96	12.96	3.14	24.50	7.31	0.66	0.29	0.28
TIBB[a]	...	...	...	...	...	...	...	...	1.28	0.35	0.61
TIBB[b]	8.94	3.23	-6.62	-9.15	-2.61	-4.29	-6.08	-77.31	1.36	0.38	0.63
TIBB[c]	8.94	3.23	8.58	-11.32	3.25	-0.60	6.35	-2.79	1.17	0.39	0.59
TIBB[d]	9.02	3.29	17.92	-1.07	10.07	7.15	15.27	27.99	1.05	0.35	0.55
TIBB[e]	0.00	0.00	12.64	-29.26	13.27	0.87	9.75	40.15	1.12	0.45	0.53
TIBB[f]	8.66	3.03	26.75	0.11	21.52	15.64	24.00	34.85	0.94	0.35	0.48
TMGO[a]	...	...	...	...	...	...	...	...	1.00	0.34	0.51
TMGO[b]	10.34	2.15	9.92	0.39	1.47	1.14	7.46	-40.36	0.90	0.34	0.50
TMGO[c]	10.34	2.15	10.27	2.54	-0.04	0.73	7.60	-11.30	0.90	0.33	0.51
TMGO[d]	10.40	2.18	7.46	3.28	3.73	3.59	6.40	11.47	0.93	0.33	0.49
TMGO[e]	0.00	0.00	8.78	10.50	27.14	21.73	12.09	58.54	0.91	0.30	0.37
TMGO[f]	9.95	2.05	20.78	25.41	23.90	24.35	21.73	38.83	0.79	0.25	0.39
TROM[a]	...	...	...	...	...	...	...	...	1.14	0.56	0.58
TROM[b]	9.51	2.37	16.66	-6.06	4.13	-0.89	10.36	-42.53	0.95	0.59	0.56
TROM[c]	9.51	2.37	21.13	3.69	-0.43	1.53	14.02	-9.70	0.90	0.54	0.58
TROM[d]	9.61	2.40	16.77	3.76	-3.01	0.18	10.83	10.14	0.95	0.54	0.60
TROM[e]	0.00	0.00	16.53	3.26	5.94	4.64	12.34	45.37	0.95	0.54	0.55
TROM[f]	9.15	2.28	25.66	10.71	12.19	11.47	20.59	22.78	0.85	0.50	0.51
USUD[a]	...	...	...	...	...	...	...	...	0.99	0.49	0.81
USUD[b]	7.47	2.07	7.82	-0.26	-1.48	-1.15	3.40	-24.18	0.91	0.49	0.82
USUD[c]	7.47	2.07	-6.82	-0.43	1.54	1.01	-3.13	1.69	1.06	0.49	0.80

Table 7. (continued)

Site	%15	%10	%rad	%lat	%lon	%2-D	%3-D	%chi	rad	lat	lon
USUD[d]	7.49	2.09	-3.13	3.50	3.29	3.35	-0.06	26.92	1.02	0.47	0.78
USUD[e]	0.00	0.00	1.55	-0.47	7.46	5.26	3.32	49.14	0.97	0.49	0.75
USUD[f]	7.37	2.06	0.22	2.72	6.91	5.77	2.85	21.04	0.99	0.48	0.75
WEST[a]	...	...	...	...	...	...	...	...	1.12	0.31	0.60
WEST[b]	10.73	2.72	3.51	-10.74	-5.83	-6.88	0.62	-71.85	1.08	0.34	0.63
WEST[c]	10.73	2.72	5.53	2.25	-1.71	-0.89	3.77	-32.20	1.06	0.30	0.61
WEST[d]	10.78	2.74	10.67	11.35	0.03	2.30	8.35	9.44	1.00	0.27	0.60
WEST[e]	0.00	0.00	28.14	1.70	19.16	15.19	24.46	54.55	0.80	0.30	0.49
WEST[f]	10.66	2.71	28.31	14.30	19.26	18.19	25.47	27.90	0.80	0.27	0.48
WHC1[a]	...	...	...	...	...	...	...	...	1.10	0.33	0.52
WHC1[b]	9.77	2.78	20.23	-4.25	-3.87	-3.98	13.81	-45.74	0.88	0.34	0.54
WHC1[c]	9.77	2.78	15.68	-6.23	-7.15	-6.88	9.76	-26.49	0.93	0.35	0.56
WHC1[d]	9.83	2.82	18.63	-1.95	1.08	0.18	13.85	10.74	0.90	0.34	0.51
WHC1[e]	0.00	0.00	22.13	7.40	12.02	10.64	19.23	56.24	0.86	0.31	0.46
WHC1[f]	9.67	2.77	33.22	17.49	21.58	20.36	29.93	36.60	0.73	0.27	0.41
WHI1[a]	...	...	...	...	...	...	...	...	1.06	0.34	0.53
WHI1[b]	9.77	2.54	14.35	-5.30	-4.38	-4.65	8.95	-47.67	0.91	0.36	0.55
WHI1[c]	9.77	2.54	16.42	1.06	-7.75	-5.29	10.18	-9.85	0.89	0.34	0.57
WHI1[d]	9.82	2.57	17.59	-0.44	-4.12	-3.07	11.67	14.21	0.87	0.34	0.55
WHI1[e]	0.00	0.00	21.93	15.27	16.83	16.38	20.43	61.88	0.83	0.29	0.44
WHI1[f]	9.48	2.52	32.56	19.89	19.81	19.83	28.98	41.28	0.71	0.27	0.43
YAR1[a]	...	...	...	...	...	...	...	...	0.76	0.24	0.46
YAR1[b]	10.93	3.13	-7.02	-10.41	-2.08	-3.89	-6.04	-70.81	0.81	0.26	0.47
YAR1[c]	10.93	3.13	-2.94	-13.32	-2.51	-4.89	-3.56	-45.81	0.78	0.27	0.47
YAR1[d]	10.97	3.16	-2.27	-13.20	-1.03	-3.71	-2.73	-9.68	0.78	0.27	0.46
YAR1[e]	0.00	0.00	1.23	-10.36	-4.92	-6.09	-1.15	32.66	0.75	0.26	0.48
YAR1[f]	10.78	3.09	-0.65	-11.38	-1.33	-3.53	-1.57	-20.52	0.76	0.27	0.47
YELL[a]	...	...	...	...	...	...	...	...	0.89	0.20	0.34
YELL[b]	12.22	2.38	7.04	-10.04	-2.59	-4.65	5.03	-79.53	0.83	0.22	0.35
YELL[c]	12.22	2.38	5.96	-10.58	5.15	0.66	5.07	-48.19	0.84	0.22	0.32
YELL[d]	12.23	2.39	10.05	-14.60	1.40	-3.16	7.76	-14.77	0.80	0.23	0.34
YELL[e]	0.00	0.00	13.59	1.22	10.24	7.72	12.61	42.49	0.77	0.20	0.31
YELL[f]	12.09	2.35	12.22	15.97	19.02	18.19	13.17	3.11	0.78	0.17	0.28
ZWEN[a]	...	...	...	...	...	...	...	...	1.00	0.37	0.58
ZWEN[b]	12.62	4.00	24.17	-8.25	15.66	8.08	18.62	-36.71	0.76	0.40	0.49
ZWEN[c]	12.62	4.00	27.95	15.62	15.15	15.29	23.63	16.84	0.72	0.31	0.49
ZWEN[d]	12.67	4.02	29.58	11.13	6.86	8.08	21.98	30.43	0.70	0.33	0.54
ZWEN[e]	0.00	0.00	17.04	7.31	17.30	14.28	16.14	53.96	0.83	0.34	0.48
ZWEN[f]	12.09	3.90	24.26	14.20	25.50	22.05	23.54	34.08	0.76	0.32	0.43

Percent improvement is measured relative to the current JPL strategy. Therefore a positive number indicates improvement over this strategy and a negative number indicates degradation. Column abbreviations are %15, percent of measurements taken below 15°; %10, percent of measurements taken below 10°; %rad, percent improvement in repeatability of the radial component of the position vector; %lat, percent improvement in repeatability of the latitude component of the position vector; %lon, percent improvement in repeatability of the longitude component of the position vector; %2-D, percent improvement in repeatability of the horizontal component of the position vector ($= \sqrt{\%\text{lat}^2 + \%\text{lon}^2}$); %3D, percent improvement in the position vector ($= \sqrt{\%\text{rad}^2 + \%\text{lat}^2 + \%\text{lon}^2}$); %chi, percent improvement in chi square of position vector; rad, repeatability, in centimeters, of the radial component of the position vector; lat, repeatability, in centimeters, of the latitude component of the position vector; lon, repeatability, in centimeters, of the longitude component of the position vector. All comparisons are done with respect to current JPL estimation strategy.

[a]Current JPL estimation strategy
[b]Nominal homogeneous estimation strategy
[c]Constant gradient estimation strategy
[d]Nominal inhomogeneous estimation strategy
[e]Tuned 15° strategy
[f]Tuned inhomogeneous estimation strategy

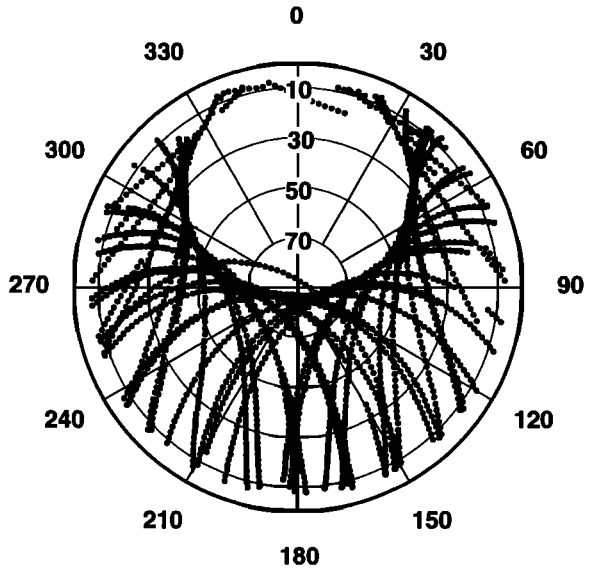

Figure 9. Azimuth-elevation distribution of observations by the ONSA GPS receiver during October 14, 1995. North is 0°, east is 90°.

precision and accuracy for precise point positioning. The improvement in precision is inferred from a significant reduction in position repeatabilities. The improvement in accuracy is inferred from direct comparisons of ZWD estimates with the independent technique of water vapor radiometry. Although the improvement appears to be robust, it can vary considerably from site to site. Of particular concern are the four sites (ONSA, REYK, STJO, and YAR1) that seem to be adversely affected by the presence of the gradient model. An inspection of Table 7 reveals that it is not the presence of the gradient model that causes a degradation in repeatability compared to the current JPL estimation strategy but, rather, the reduction in elevation angle cutoff value. For these sites (and for almost all other tested sites) the tuned inhomogeneous strategy is far superior to the nominal homogeneous strategy. At low-elevation angles the impact of the gradients on the observable becomes very significant, and prevailing gradients will have systematic effects on the estimation of geodetic quantities. The emerging rule is that a reduction in elevation angle cutoff value from 15° or 20° to the 5°- 10° range should be accompanied by modeling the troposphere gradient, especially if good horizontal repeatability is desired.

Variants of the constant gradient strategy were employed by *MacMillan* [1995] for VLBI data processing. We tested this strategy in order to provide an alternative strategy for those who do not use stochastic models. This strategy could be employed to observe the hydrostatic gradient in the troposphere, but it is clearly unsuitable for the observation of moisture gradients because of their short timescales. Overall, this strategy proved an able performer, although on average, it is inferior to the tuned inhomogeneous strategy. The full performance statistics are provided in Table 7. Obviously, site-specific tuning of estimation strategy and mapping function will provide the best performance, but a nonuniformity of the estimation strategy would probably not be tolerated in most operational processes.

Many factors contribute to the variety of responses to the tuned estimation strategy. At this time we can only speculate that factors such as local multipath and phase center pattern may affect the results in an unpredictable way. We note that the ONSA GPS antenna is covered with a radome and that the data for our experiments were collected during the northern hemisphere winter, when snow and ice can affect the phase pattern of the GPS antenna at some sites. Some antennae are more noisy at low-elevation angles than others, etc. The study of errors introduced by the simple mapping function we employed here might be an interesting and fruitful investigation. For example, *Chen and Herring*

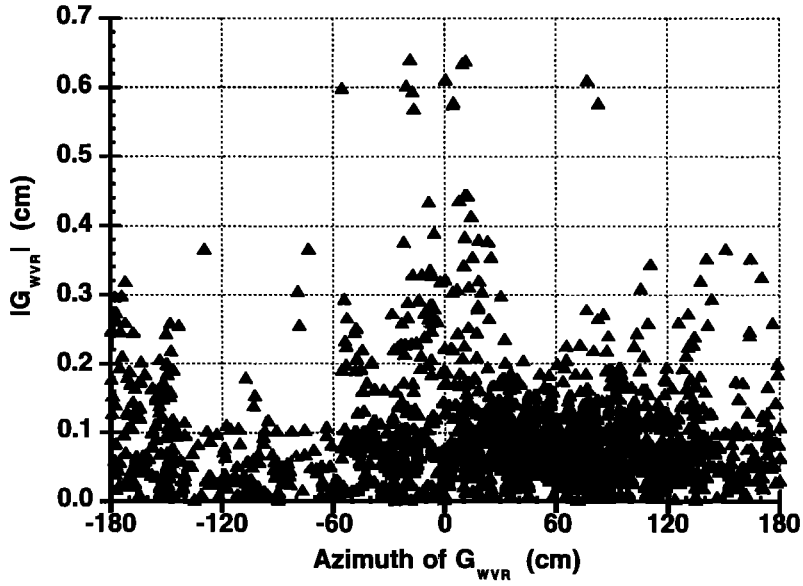

Figure 10. Magnitude and azimuth of the WVR-based gradients. North is 0°, east is 90°.

[1997] proposed an inhomogeneous mapping function that should be more accurate than (1), especially at low elevation angles.

Biases associated with the change of elevation angles cutoff are unavoidable, for most receivers. We have contributed here one more piece of evidence (to an already large collection) linking the reduction in elevation angle cutoff to improved accuracy (Tables 2 and 5). It is noteworthy that the presence of the gradient model tends to reduce these biases.

Note that recent analysis carried out at JPL found that the estimation of atmosphere gradients with the tuned 15° strategy at all the sites participating in the global determination of GPS orbits and clocks resulted in 10% improvement to the median orbit repeatabilities of all satellites. The tuned inhomogeneous strategy gave essentially the same results because most IGS sites do not track well below 15°. As a result, starting August 24, 1997, the IGS Analysis Center at JPL has switched its estimation strategy for the global solution and for point positioning to the tuned 15° strategy (IGS report 4112, http://igscb.jpl.nasa.gov/mail, 1997).

The second part of this paper is dedicated to the validation of a new GPS product: estimates of troposphere gradients. We have shown that GPS-based estimates of troposphere gradients seem to capture accurately the direction (azimuth) of significant moisture gradients. The magnitude of the gradients is captured less accurately, with errors at the 60% level. The primary error source in our data processing is the crude treatment of the hydrostatic delay which, of course, does not remain exactly constant over contiguous 12-hour intervals. This must be a major contributor to the large difference in magnitude between the GPS- and the WVR-based gradients. Another major error source is the inability of the GPS estimates to track fast-changing gradients due to the tight time correlation imposed by the random walk variance of 0.3 mm/$\sqrt{\text{h}}$. Relaxing the random walk sigma results, typically, in improved agreement in magnitude of large gradients with the WVR but at the cost of lower linear correlation overall and increased discrepancy in azimuth.

Errors in our method to extract gradient estimates from the line-of-sight WVR delay could also have contributed to degradation in the comparison statistics. In particular, the relatively high elevation angle cutoff of the WVR observations may have affected the accuracy of the retrieval. It also implies that the GPS senses a rather different atmosphere than the WVR does. An increase in the GPS elevation angle cutoff to 15° did not improve the agreement. Site-specific error sources, such as multipath and antenna characteristics, may be another factor that strongly impacts our comparison. The inhomogeneous mapping function, $m_\Delta(e)\cot e$, may also introduce significant errors at low-elevation angles, as indicated by *Chen and Herring* [1997]. A systematic error may be present in the GPS solution due to the azimuthally asymmetric distribution of observations (Figure 9), especially in light of the fact that the dominant gradients, as observed by the WVR, are in the north-south direction (Figure 10) and the consequent dominance of the G_N component of the gradient relative to G_E (Figure 8). However, the similarity in formal errors between the two GPS-based gradient components and the good agreement in azimuth with the WVR-based gradients suggest no ill effects on the GPS estimates due to this asymmetry.

It is important that future comparisons will be carried out at other sites in order to construct a reliable error budget for the estimation of troposphere gradients. An alternative method for the validation of the GPS gradient estimate is to deploy a dense network of GPS receivers around the test receiver and to use the ZWD from each receiver to construct the local wet delay field. We expect the ability to retrieve troposphere gradients to improve as new receivers and antennae are designed to produce high-quality observations at low-elevation angles.

Acknowledgments. We wish to thank Per Jarlemark and Jan Johansson of the Onsala Space Observatory for supplying the Onsala WVR data. We also wish to thank the reviewers of this paper for their excellent suggestions and comments. The work described in this paper was carried out in part by the Jet Propulsion Laboratory, California Institute of Technology, under contract with the National Aeronautics and Space Administration.

References

Bar-Sever, Y. E., Strategies for near real time estimates of precipitable water vapor, in *International GPS Service for Geodynamics 1996 Analysis Center Workshop,* edited by R. E. Nielan, P. A., Van Scoy, and Z. F. Zumberge, pp. 165-175, *JPL Publ. 96-23,* Pasadena, Calif., 1996.

Bar-Sever, Y. E., and P. M. Kroger, Strategies for GPS-based estimates of troposphere delay, in *ION GPS-96,* pp. 615-623, Institute of Navigation, Alexandria, Virginia, 1996.

Bevis, M., S. Businger, S. Chiswell, T. A. Herring, R. A. Anthes, C. Rocken, and R. H. Ware, GPS meteorology: mapping zenith wet delays onto precipitable water, *J. Appl. Meteorol., 33*(3), 1994.

Businger, S., S. R. Chiswell, M. Bevis, J. Duan, A. Anthes, C. Rocken, R. H. Ware, M. Exner, T. VanHove, and F. S. Solheim, The promise of GPS in atmospheric monitoring, *Bull. Am. Meteorol. Soc., 77*(1), 1996.

Chen, G. and T. H. Herring, Effects of atmospheric azimuthal asymmetry on the analysis of space geodetic data, *J. Geophys. Res., 102,* 20,489-20,502, 1997.

Davis, J. L., T. A. Herring, I. I. Shapiro, A. E. E. Rogers, and G. Elgered, Geodesy by radio interferometry: effects of atmospheric modeling errors on estimates of baseline length, *Radio Sci., 20,* 1593-1607, 1985.

Davis, J. L., G. Elgered, A. E. Niell, and C. E. Kuehn, Ground-based measurements of the gradients in the "Wet" radio refractivity of air, *Radio Sci, 28,* 1003-1018, 1993.

Duan, J., et al., GPS meteorology: direct estimation of the absolute value of precipitable water, *J. Appl. Meteorol., 35*(6), 1996.

Gardner, C. S., Correction of laser tracking data for The effects of horizontal refractivity gradients, *Appl. Opt., 16,* 2427-2432, 1977.

Heflin, M. B., M. M. Watkins, and D. Dauger, GPS time Series: noise characteristics based on 55405 station-days

(abstract), *Eos Trans. AGU, 77*(17), Spring Meet. Suppl., S72, 1996.

Heflin, M., D. Jefferson, Y. Vigue, F. Webb, J. Zumberge, D. Argus, and G. Blewitt, Vertical rates determined with the Global Positioning System (abstract), *Eos Trans. AGU, 75*(16), Spring Meet. Suppl., 104, 1994.

Herring, T. A., Modeling atmospheric delays in the analysis of space geodetic data, in Refraction of Transatmospheric Signals in Geodesy, vol. 36, edited by J. C. Munck and T. A. Spoelstra, pp. 157-164, Neth. Geod. Comm. Publ. Geod., Delft, 1992.

Lanyi, G., Tropospheric delay effects in radio interferometry, April-June 1984, *TDA prog. rep. 42-78,* Jet Propul. Lab., Pasadena, Calif., August 15, 1984.

MacMillan, D. S., Atmospheric gradients from very long baseline interferometry observations, *Geophys. Res. Lett., 22,* 1041-1044, 1995.

MacMillan, D. S., and C. Ma, Evaluation of very long baseline interferometry atmospheric modeling improvements, *J. Geophys. Res., 99,* 637-651, 1994.

Niell, A. E., Global mapping functions for the atmospheric delay at radio wavelengths, *J. Geophys. Res., 101,* 3227-3246, 1996.

Runge, T. F., P. M. Kroger, Y. E. Bar-Sever, and M. Bevis, Accuracy evaluation of ground-based GPS estimates of precipitable water vapor (abstract), *Eos Trans., AGU, 76* (46), Fall Meet. Suppl., F146, 1995.

Saastamoinen, J., Atmospheric correction for the troposphere and stratosphere in radio ranging of satellites, in *The Use of Artificial Satellites for Geodesy, Geophys. Monogr. Ser.,* vol. 15, edited by S. W. Henriksen et al., pp. 247-251, AGU, Washington, D.C., 1971.

Ware, R., C. Alber, C. Rocken, and F. Solheim, Sensing integrated water vapor along GPS ray paths, *Geophys. Res. Lett., 24,* 417-420, 1997.

Wolfe, D. E., and S. I. Gutman, Comparing changes in GPS preciptable water vapor to vertical profiles of precipitable water vapor (abstract), *Eos Trans. AGU, 75*(44), Fall Meet.Supp., 174, 1994.

Zumberge, J. F., M. B. Heflin, D. C. Jefferson, M. M. Watkins, and F. H. Webb, IGS Analysis Center 1994 annual report, *JPL Publ. 95-18,* Jet Propul. Lab., Pasadena, Calif., September 1, 1995.

Zumberge, J. F., M. B. Heflin, D. C. Jefferson., M. M. Watkins, and F. H. Webb, Precise point positioning for the efficient and robust analysis of GPS data from large networks, *J. Geophys. Res., 102,* 5005-5017, 1997.

Y. E. Bar-Sever and P. M. Kroger, M.S. 238-600, Jet Propulsion Laboratory, Pasadena, CA 91109. (e-mail: yeb@cobra.jpl.nasa.gov)

J. A. Borjesson, Onsala Space Observatory, Chalmers University of Technology, Onsala, S-43992, Sweden. (e-mail: ajb@oso.chalmers.se)

(Received July 3, 1997; revised November 7, 1997; accepted December 3, 1997.)